Wound-response jasmonate dynamics in the primary vasculature

Hugo Morin[1,2] (iD), Aurore Chételat[3] (iD), Stéphanie Stolz[3] (iD), Laurence Marcourt[1,2] (iD), Gaëtan Glauser[4] (iD), Jean-Luc Wolfender[1,2] (iD) and Edward E. Farmer[3] (iD)

[1]Institute of Pharmaceutical Sciences of Western Switzerland, University of Geneva, CMU, 1206, Geneva, Switzerland; [2]School of Pharmaceutical Science, University of Geneva, CMU, 1206, Geneva, Switzerland; [3]Department of Plant Molecular Biology, University of Lausanne, 1015, Lausanne, Switzerland; [4]Neuchâtel Platform of Analytical Chemistry, University of Neuchâtel, 2000, Neuchâtel, Switzerland

Summary

- The links between wound-response electrical signalling and the activation of jasmonate synthesis are unknown. We investigated damage-response remodelling of jasmonate precursor pools in the *Arabidopsis thaliana* leaf vasculature.
- Galactolipids and jasmonate precursors in primary veins from undamaged and wounded plants were analysed using MS-based metabolomics and NMR. In parallel, DAD1-LIKE LIPASEs (DALLs), which control the levels of jasmonate precursors in veins, were identified.
- A novel galactolipid containing the jasmonate precursor 12-oxo-phytodienoic acid (OPDA) was identified in veins: *sn*-2-*O*-(*cis*-12-oxo-phytodienoyl)-*sn*-3-*O*-(β-galactopyranosyl) glyceride (*sn*-2-OPDA-MGMG). Lower levels of *sn*-1-OPDA-MGMG were also detected. Vascular OPDA-MGMGs, *sn*-2-18:3-MGMG and free OPDA pools were reduced rapidly in response to damage-activated electrical signals. Reduced function *dall2* mutants failed to build resting vascular *sn*-2-OPDA-MGMG and OPDA pools and, upon wounding, *dall2* produced less jasmonoyl-isoleucine (JA-Ile) than the wild-type. DALL3 acted to suppress excess JA-Ile production after wounding, whereas *dall2 dall3* double mutants strongly reduce jasmonate signalling in leaves distal to wounds.
- LOX6 and DALL2 function to produce OPDA and the non-bilayer-forming lipid *sn*-2-OPDA-MGMG in the primary vasculature. Membrane depolarizations trigger rapid depletion of these molecules. We suggest that electrical signal-dependent lipid phase changes help to initiate vascular jasmonate synthesis in wounded leaves.

Introduction

Sudden cell rupture when the primary vasculature is severed by feeding herbivores triggers the production of electrical signals called slow-wave potentials (SWPs; Stahlberg *et al.*, 2006; Kurenda *et al.*, 2019). In Arabidopsis, these signals are propagated from leaf to leaf at apparent velocities of *c.* 8 centimetres per minute to initiate the synthesis of jasmonates (Mousavi *et al.*, 2013). Jasmonates (Wasternack & Feussner, 2018) have potent activities related to plant defence. For instance, jasmonoyl-isoleucine (JA-Ile; Staswick & Tiryaki, 2004; Fonseca *et al.*, 2009) acts as a highly selective ligand, initiating the de-repression of a large array of defence genes (Howe *et al.*, 2018) leading to augmented defences against numerous herbivores (Erb & Reymond, 2019; Wang *et al.*, 2019). A key feature of JA-Ile in Arabidopsis leaves is that it is not stored ready for use. Instead, the synthesis of this mediator in leaves is initiated upon wounding (Howe *et al.*, 2018). These features distinguish JA-Ile from one of its key precursors, the 18-carbon cyclopentenone 12-oxo-phytodienoic acid (OPDA). Several signalling functions have been proposed for OPDA (Jimenez Aleman *et al.*, 2022). For example, OPDA

and its 16-carbon homologue dinor-OPDA (dnOPDA) were proposed to control their own synthesis and/or steady-state levels (Weber *et al.*, 1997). JA-Ile synthesis is rapid and is initiated in < 3 min in undamaged leaves that are vascularly connected to wounded leaves (Chauvin *et al.*, 2013). In parallel, preformed OPDA pools are depleted rapidly in Arabidopsis leaves distal to wounds (Koo *et al.*, 2009).

Here, we attempted to identify jasmonate precursor lipids and the proteins that process them upon arrival of electrical signals in leaves distal to wounds. For this, we focused on free and bound 12-oxo-phytodienoic acid (OPDA) pools. Only a fraction of the OPDA pools in leaves is unbound, and it has been estimated that 80–90% of OPDA (and dnOPDA) in Arabidopsis leaves is esterified to galactolipids, including monogalactosylmonoacylglycerol (MGMG), monogalactosyldiacylglycerol (MGDG) and digalactosyldiacylglycerol (DGDG; Stelmach *et al.*, 2001; Ohashi *et al.*, 2005; Buseman *et al.*, 2006; Hölzl & Dörmann, 2007; Genva *et al.*, 2019). Moreover, MGDGs were proposed as substrates for jasmonate synthesis (Weber *et al.*, 1997; Lin *et al.*, 2016). Early in jasmonate production, dioxygenases add molecular oxygen into linolenic acid (18:3). In the case of pools

of free OPDA in leaves, this reaction is catalysed by LIPOXY-GENASE 6 (LOX6; Chauvin *et al.*, 2013). Either 18:3 bound to galactolipids is oxygenated directly by LOXs to provide precursors for jasmonate synthesis, or free 18:3 derived from galactolipids is oxygenated to generate OPDA precursors. There is evidence for the former mechanism: Fatty acid oxygenation to produce jasmonates can occur in wounded leaves before the release of free linolenic acid from parent lipids (Nilsson *et al.*, 2012). In both cases, jasmonate synthesis requires the action of a specific lipase(s) to cleave the galactolipid substrate. These lipases are present in undamaged plants since, in Arabidopsis leaves, the enzymes necessary for rapid, wound-response jasmonate synthesis are preformed (Kimberlin *et al.*, 2022). In addition to studying galactolipid/OPDA remodelling upon wounding, we sought the lipases which help initiate jasmonate synthesis when electrical signals arrive in leaves distal to wounds.

Initially, the lipase gene (*DEFECTIVE IN ANTHER DEHISCENCE 1, DAD1*) was identified as necessary for jasmonate-dependent male fertility in *Arabidopsis* (Ishiguro *et al.*, 2001). This enzyme is a member of the Arabidopsis phospholipase A (PLA) superfamily (Ryu, 2004), which contains several *DAD1-like LIPASEs* (*DALLs*; Ruduś *et al.*, 2014). Much evidence that DALLs operate in jasmonate synthesis in vegetative tissues has accumulated (e.g. Ryu, 2004; Yang *et al.*, 2007; Seo *et al.*, 2009; Ellinger *et al.*, 2010; Ruduś *et al.*, 2014; Lin *et al.*, 2016; Wang *et al.*, 2018; Kimberlin *et al.*, 2022), although the exact DALLs that initiate jasmonate synthesis in leaves in response to wounding remain to be identified. However, Ellinger *et al.* (2010) produced the *c1x11* mutant from individual T-DNA insertion mutations in DALLs 1–4. This quadruple mutant displayed reduced JA and OPDA accumulation in undamaged leaves and in leaves that had been wounded. We deconvoluted *c1x11* in attempts to delineate the roles of individual DALLs in electrical signal-dependent galactolipid remodelling. Leaf veins in *A. thaliana*, and in particular cells associated with the xylem and phloem, have a high capacity for jasmonate synthesis (Hause *et al.*, 2003; Chauvin *et al.*, 2016). To overcome some of the complexity of early steps in jasmonate synthesis in whole leaves, we used vein extraction (Farmer & Kurenda, 2018) to monitor wound-response jasmonate precursor profiles with unprecedented depth. Moreover, we avoided analysing crushed tissues by extracting veins from distal leaf 13 after wounding leaf 8. In summary, the present work aimed to identify vascular galactolipid species involved in electrical signal-induced JA-Ile production and to identify the key lipases involved in this process.

Materials and Methods

Plants, growth conditions and wounding

Arabidopsis thaliana (L.) Heynh. (Columbia) were soil grown in 7 cm diameter pots on soil for 5 wk for experiments on whole leaves, or 6 wk for vein experiments. Before germination, seeds were stratified at 5° for 2 d. Growth conditions were the following: 10 h d ($100 \mu E \, s^{-1} \, m^{-2}$) with 70% humidity at 22°C during daytime and 18° at night. *lox3B* (SALK_147830), *lox4A*

(SALK_071732) and *lox6B* (SALK_083650) were from Caldelari *et al.* (2011); *lox2-1* (At3g45140) was from Glauser *et al.* (2009). The *lox2-1 lox3B lox4A* triple mutants were from Chauvin *et al.* (2013). The *glr3.3 glr3.6* double mutant was from Mousavi *et al.* (2013). The *c1x11* mutant of Ellinger *et al.* (2010) was kindly supplied by S. Berger and M. Mueller (University of Wuerzburg, Germany). T-DNA insertion mutants for *DALLs* were obtained from the Nottingham Arabidopsis Stock Centre (http://arabidopsis.info/): *DALL1* (At4g16820) SM_3_17158; *DALL2* (At1g51440) Salk_012430; *DALL2* (At1g51440) Salk_012432; *DALL3* (At2g30550) Salk_003105; *DALL4* (At1g06800) Salk_084254. Leaves were numbered chronologically starting with the oldest leaf. Wounding was performed with metal forceps. Leaf 8 was wounded by crushing 30% of the apical lamina. Distal metabolic changes were monitored in connected leaf 13. Control leaves were unwounded leaves 8–11. Injury infliction was accomplished in < 10 s, and the timing started immediately afterwards. Primary veins were extracted from expanded leaves using protocol 2 in Farmer & Kurenda (2018). Harvested fresh material was immediately snap-frozen in liquid nitrogen and stored at −80°C before analysis.

Oxylipin quantification in leaves and primary veins

Fresh leaves were ground in a pre-frozen mortar, and *c.* 25 mg of powder was weighed accurately. Primary veins were ground in pre-frozen Eppendorf tubes using a pellet pestle and *c.* 10 mg were weighed accurately. Care was taken to avoid any thawing before adding the extraction solvent. Extraction according to Glauser *et al.* (2014) used ethyl acetate: formic acid, 99.5 : 0.5 (v/v) with the addition of an internal standard solution containing $^{13}C_6$-JA-Ile. Extracts were evaporated to dryness and reconstituted in 100 μl of methanol: H_2O (70 : 30, v/v). The final concentration of the internal standard was 10 ng ml^{-1}. OPDA, JA, JA-Ile and *sn*-2-OPDA-MGMG were quantified using UHPLC–MS/MS. The measurements were carried out on two generations of the same mass spectrometer. The first system consisted of a QTRAP 4000 (AB Sciex, Darmstadt, Germany) coupled to a Dionex UltiMate 3000 quaternary RSLC system (Thermo Fisher Scientific, Waltham, MA USA) and controlled by Analyst 1.5.1, while the second was a QTRAP 6500+ (AB Sciex) coupled to an Acquity UPLC I-Class system (Waters, Milford, MA, USA) and controlled by ANALYST 1.7.1. All analyses were performed in the multiple reaction monitoring (MRM) mode with negative ionization and the following parameters (QTRAP 4000/6500+): ion spray voltage, −4500/−4500 V; curtain gas, 25/35 psi; ion source gas 1 (GS1), 45/40 psi; ion source gas 2 (GS2), 30/35 psi; source temperature, 550/500°C. MRM transitions were: JA, 209.1 > 59.0; OPDA, 291.2 > 165.1; JA-Ile, 322.2 > 130.0; JA-$^{13}C_6$Ile, 328.2 > 136.0; and *sn*-2-OPDA-MGMG, 573.4 > 291.2 (precursor ion > product ion). The MRM parameters for *sn*-2-OPDA-MGMG were optimized by direct infusion at 20 ng ml^{-1} into the mass spectrometer systems. MRM parameters of OPDA, JA, JA-Ile and $^{13}C_6$-JA-Ile were from Glauser *et al.* (2014). Separation was on a Waters UPLC BEH C18 column (2.1 × 50 mm; 1.7 μm; Waters). The injection

volume was 5 µl on the QTRAP 4000 and 1 µl on the QTRAP 6500+. The column oven temperature was 35°C. The solvent system was A = 0.05% formic acid/water and B = 0.05% formic acid/acetonitrile. The gradient flow rate was 0.4 ml min^{-1}: 5–65% B in 6.5 min, 65–100% B in 0.5 min, holding at 100% B for 2 min and reconditioning at 5% B for 3 min. Concentrations corresponding to signal-to-noise ratios of 10 represented the limit of quantification (LOQ). Due to the difference in performance between both mass analysers, LOQ were evaluated independently. On the QTRAP 4000, the LOQ was 10 pmol g^{-1} 1 fresh weight (FW) for OPDA, 1.5 pmol g^{-1} FW for JA and 1 pmol g^{-1} FW for JA-Ile. On the QTRAP 6500+, the LOQ was 1 pmol g^{-1} FW for OPDA, 0.8 pmol g^{-1} FW for JA, 0.5 pmol g^{-1} FW for JA-Ile and 4 pmol g^{-1} FW for *sn-2-*OPDA-MGMG.

UHPLC-HRMS/MS screening of free and bound OPDA/dnOPDA in primary veins

Untargeted analyses were performed on a Q-Exactive Focus mass spectrometer (Thermo Scientific, Bremen, Germany) with a heated electrospray interface (HESI-II) coupled with an ACQUITY UPLC (Waters). HESI conditions: source voltage −2.5 kV; sheath gas flow rate (N$_2$) 55; auxiliary gas flow rate 15; spare gas flow rate 3.0; capillary temperature 275°C; and S-Lens RF level 45. Detection was in negative ion mode over the *m/z* range of 120–1500 Da. Internal calibration used a mixture of caffeine, methionine–arginine−phenylalanine−alanine−acetate (MRFA), sodium dodecyl sulphate, sodium taurocholate and Ultramark 1621 (Thermo Scientific) in an acetonitrile : methanol : water (1 : 1 : 1, v/v) solution containing 1% formic acid by direct injection. Separation was on a UPLC BEH C18 column (2.1 × 100 mm; 1.7 µm; Waters) with the solvent system: A was 0.1% (v/v) formic acid in water, and B was 0.1% (v/v) formic acid in acetonitrile. The flow rate was set to 600 µl min^{-1}, and the gradient started at 5% B, increased linearly from 5% to 100% B in 17 min and held at 100% B for 1 min followed by re-equilibration at 5% of B. The injection volume was 5 µl. Screening of oxylipin forms was based on data-dependent MS/MS (MS^2) events and performed on the three most intense ions detected in full scan MS. The MS/MS isolation window width was 1 Da. Stepped normalized collision energy (NCE) was set to 15, 30 and 45 units. Full scans were acquired at a resolution of 35 000 full width at half maximum (FWHM) at *m/z* 200 and MS/MS scans at 17 500 FWHM both with an automatically determined maximum injection time.

Isolation of dnOPDA-MGMGs and OPDA-MGMGs

Expanded WT leaves were wounded by crushing the apical 30% with forceps. After 30 min incubation in the light, leaves were harvested and frozen immediately in liquid nitrogen then ground in a frozen mortar. A large-scale methanol extract was prepared from 250 g of leaves by extracting three times with 1.5 l of MeOH by sonication for 1 h followed by filtration to remove the leaf debris from the solution. After drying under nitrogen, this yielded 4.2 g of crude leaf extract. To ensure the presence of OPDA-MGMGs, which are poorly detected by both UV and ELSD detectors, an aliquot of this sample was analysed by UHPLC-HRMS/MS using the same conditions as those used for the UHPLC-HRMS/MS screening (as mentioned in the previous section).

The methanol extract was fractionated by preparative-scale MPLC chromatography using UV detection after a geometrical gradient transfer from analytical HPLC conditions (Challal *et al.*, 2015). The fractionation was on a preparative Interchim HP C18 column (235 × 63 mm I.D.; 15 µm; Interchim, Montluçon, France). The mobile phases consisted of a mixture of: A = 0.1% formic acid/water, B = 0.1% formic acid/acetonitrile. Gradients were run at a flow rate of 50 ml min^{-1} with the following steps: 10–65% B in 170 min, 65–100% B in 20 min, holding at 100% B for 30 min. Injection of crude extract (4.2 g) was performed by dry loading according to Challal *et al.* (2015). MPLC-UV separation was monitored at 220 nm. Since the various oxylipins of interest could not be detected by UV, an elution zone (90–120 min, corresponding to F96-F129) corresponding to the fractions of interest was evaluated by calculating expected retention times at the preparative level, based on retention times obtained at the analytical level. Each of these fractions (F) was checked for the presence of OPDA-MGMGs and dnOPDA-MGMGs by UHPLC-HRMS/MS. F97 contained pure *sn-2-*dnOPDA-MGMG. F116 was a mixture of compounds. F118 and F119 were found to contain OPDA-MGMGs and were submitted to micro-fractionation using UHPLC-DAD. Separation was on a Waters Acquity UPLC combined with Fraction Manager module (Waters). OPDA-MGMGs isolation was carried out on a Waters UPLC BEH C18 column (2.1 × 50 mm I.D.; 1.7 µm). The solvent system consisted of A = 0.1% formic acid/water and B = 0.1% formic acid/acetonitrile. Gradients were run at flow rates of 600 µl min^{-1} with the following steps: 30–38% B in 3.5 min, 38–100% B in 0.1 min, holding at 100% B for 0.4 min and reconditioning at 30% B for 2 min. Instrument control and data acquisition were achieved using Empower software (Waters). F118 and F119 were both repetitively injected 40 times with injection volume of 5 µl at 2.5 mg ml^{-1}. OPDA-MGMGs were successfully monitored at 220 nm, and the collection time was set between 2.60 and 3.11 min. The collection time corresponded to 300 µl per fraction. Fractions were then merged and yielded 20 µg of pure *sn-1-*OPDA-MGMG.

Structural elucidation using NMR

NMR spectroscopic data were recorded on a Bruker Avance NEO 600 MHz NMR spectrometer equipped with a QCI 5 mm Cryoprobe and a SampleJet automated sample changer (Bruker BioSpin, Rheinstetten, Germany). Chemical shifts (δ) are measured in parts per million (ppm) and coupling constants (*J*) are reported in Hertz (Hz). Complete assignments were performed based on two-dimensional experiments (COSY, NOESY, HSQC and HMBC). See Supporting Information Notes S1 for details concerning individual MGMGs.

Vein extract preparation for 18:3-MGMG characterization

A large-scale methanolic extract was prepared from veins isolated from *c.* 250 undamaged WT rosettes (6 wk old). Veins were isolated using protocol 2 in Farmer & Kurenda (2018). From each rosette, *c.* 8 veins could be harvested in less than a minute and snap-frozen immediately in liquid nitrogen. Vein extraction was conducted at the analytical scale (10 veins per tube, 200 times) using the bead extraction protocol in Glauser *et al.* (2014). Samples were extracted twice in MeOH and dried down under nitrogen. The pooling of all these samples yielded 6 mg of dry extract corresponding to a total of 1.8 g FW (vein material). The presence of 18:3-MGMG in this extract was verified using the same conditions as those presented for UHPLC-HRMS screening (as mentioned in the previous section).

HPLC-DAD micro-fractionation of vein extract and isolation of *sn*-2-18:3-MGMG

The methanol extract from veins was fractionated on an Infinity 1260 II (Agilent, Santa Clara, CA, USA) HPLC-DAD system after a geometrical gradient transfer based on analytical HPLC conditions (Challal *et al.*, 2015). Fractionation was carried out on an Xbridge RP C18 column (250 × 10 mm I.D.; 5 μm; Waters). The solvent system consisted of A = 0.1% formic acid/water and B = 0.1% formic acid/acetonitrile. Gradients were run at a flow rate of 4.7 ml min^{-1} with the following steps: 5% B for 2.7 min, 5–100% B in 55 min, holding at 100% B for 10 min. Fractions of 700 μl were collected in 96-well plates (2 ml wells; VWR, Leuven, Belgium). The methanol extract was concentrated at 4 mg ml^{-1} in pure MeOH and injected three times consecutively. The fractions collected in three 96-well plates were verified according to the UHPLC-HRMS/MS programme described above. *Sn*-2-MGMG-18:3 was confirmed in fractions F38, F39 and F40 for all three plates. Each fraction was pooled into a single vial and subjected to NMR analysis.

JAZ10 expression

Total RNA was extracted from leaves (Oñate-Sánchez & Vicente-Carbajosa, 2008). One μg total RNA was copied into cDNA with the M-MLV reverse transcriptase, RNase H Minus, Point Mutant (Promega) following the manufacturer's instructions. Quantitative PCR was performed with an Applied Biosystems QuantStudio 3 Real-Time PCR System (Thermo Fisher Scientific, Reinach, Switzerland) using methods described by Gfeller *et al.* (2011). The mixture contained 0.2 mM dNTPs, 2.5 mM MgCl$_2$, 0.5 × SYBR Green I (Invitrogen, Thermo Fisher Scientific), 30 nM ROX reference dye (Thermo Fisher Scientific), 0.5 units GoTaq polymerase (Promega) and 0.25 mM of each primer (Microsynth AG, Balgach, Switzerland), in a final volume of 20 μl. PCR: 2 min initial denaturation step at 95°C, then 40 cycles of 10 s at 95°C, 30 s at 60°C and 30 s at 72°C. Data were analysed with the $2^{-\Delta\Delta C_T}$ method. Primers for the reference gene *UBC21* (*UBIQUITIN-CONJUGATING ENZYME 21*; AT5G25760) and *JAZ10* (*JASMONATE ZIM-DOMAIN 10*; AT5G13220) were from Gfeller *et al.* (2011).

Characterization of *dall* mutants

Primers for *dall* genotyping are given in Table S1. Relative levels of *DALL2* and *DALL3* transcripts in the WT, *dall2(30)* and *dall3* were estimated using qPCR. The primers used for *DALL2* were: Forward: 5′-AGACAAGCATCACCGTGACA-3′; Reverse: 5′-GGTCCCGAGAAGGAGAAAAC-3′. The primers used for *DALL3* were as follows: Forward: 5′-TGGATCATCAGAACTCGCCG-3′; Reverse: 5′-CACTAGCGCATGGTCTCTCC-3′. qPCR was performed under the same conditions and with the same reference gene as for *JAZ10* expression. The plants used were 3 wk old.

Production of *dall2c dall3c* using CRISPR-Cas9

Using the CRISPR guide RNA design tool (https://benchling.com/), three guide RNA (gRNA) sequences were designed for *DALL2* and for *DALL3* and synthesized by Microsynth AG (Balgach, Switzerland). The gRNAs were as follows: *DALL2* gRNA 1: gatcctcactctaaatactg; 2: gcacagtcacttatctcgaa; 3: gagctacgcgcacgtcggcg. *DALL3* guide 4: tcgcctcgagcgagaaaggc; 5: gatcccgcttccaaatactg; 6: attaagcgcgtacgatatag. gRNAs were cloned separately into six primary entry vectors (pRU41-46) containing the promoters pU3 or pU6.50 following Ursache *et al.* (2021). Next, the six gRNAs were assembled into an intermediate vector (pSF280; Ursache *et al.*, 2021) using Goldengate cloning. Finally, all six gRNAs with their independent promoters were assembled in a destination vector expressing Cas9i driven by the promoter pEC1.2 (pRU294). The resulting clones were sequence-verified (Microsynth AG). Transgenic plants were generated by transformation using the floral dipping. Transgenics were screened in T1 based on red seed coat fluorescence using a MZ16 FA microscope (Leica, Wetzlar, Germany). Homozygous or heterozygous *dall2* and *dall3* lines were selected using PCR and confirmed by sequencing (Microsynth AG). In T2, to remove Cas9i, non-fluorescent seeds were selected. The mutations in the double mutant *dall2c dall3c* were characterized by sequencing.

DALL2 protein localization

DALL2promoter::DALL2 genomic coding sequences were amplified from the JAtY TAC-Based Arabidopsis genomic DNA library (from the Nottingham Arabidopsis Stock Centre, http://arabidopsis.info/) with primers containing XmaI and KpnI sites using CloneAmp HIFI PCR premix (Takara Bio, Mountain View, CA, USA). The fragment (4.58 kbp) was amplified with the following primers: Forward 5′-GTATAGAAAAGTTGGGTACCCATCCAAAAAGTACTTGCT-3′; Reverse 5′-TTTAAACCCACAACGACTCCCGGGACAAGTTTGTACA-3′. The underlined sequences represent XmaI and KpnI sites, respectively. Amplified DNA was inserted into pUC57-L4-Kpn1/XmaI-R1 with In-Fusion HD Enzyme Premix (Takara Bio,

Mountain View, CA, USA) and recombined with pEN-L1-GUS-Plus-L2 (Acosta *et al.*, 2013) and the destination vector pED-O097pFR7m24GW (Chauvin *et al.*, 2013). The WT was transformed by floral dipping and transgenic lines were selected with FAST technology (Shimada *et al.*, 2010).

β-glucuronidase (GUS) staining

Expanded leaves of 3.5-wk-old *DALL2-GUS* expressing plants were fixed in 90% (v/v) acetone for 30 min on ice and then washed two times for 5 min with 50 mM sodium phosphate buffer (pH 7.2). Rosettes were then stained in 10 mM Na_2EDTA, 0.5 mM $K_4Fe(CN)_6$, 0.5 mM $K_3Fe(CN)_6$, 0.1% (v/v) Triton X-100, 0.5 mg ml^{-1} X-Gluc and 50 mM sodium phosphate buffer pH 7.2, which was vacuum infiltrated 5 times each for 10 min. Staining was in the dark at 37°C overnight. After staining, rosettes were washed in 70% EtOH. Images were obtained with a VHX-6000 digital microscope (Keyence, Mechelen, Belgium).

Primary veins from 5.5 wk-old plants were extracted according to Farmer and Kurenda (2018) and stained for 45 min as above. After the 70% EtOH wash, veins were dehydrated in absolute EtOH and then embedded in Technovit 7100 resin (Haslab GmbH, Ostermundigen, Switzerland) following the manufacturer's instructions. Transversal sections (5 μm thick) were made on a RM2255 microtome (Leica, Wetzlar, Germany), mounted in water and photographed with a Thunder DM6B microscope (Leica).

Statistical analyses

Pair-wise statistical significance was evaluated with Student's *t*-tests. GraphPad Prism 8 (GraphPad Software Inc., San Diego, CA, USA) was used for displaying quantitative data. In biochemical assays, data below the limit of quantitation (LOQ) were not used for statistical analyses.

Results

Jasmonate levels and dynamics in primary veins vs surrounding tissues

Koo *et al.* (2009) found that damaging Arabidopsis leaves led to rapid declines in OPDA levels in undamaged leaves on the same plant. To determine whether this was also the case in veins, we measured OPDA in the primary veins and in surrounding tissues (herein termed the 'sheath') of unwounded or wounded wild-type (WT) leaves. Resting levels of OPDA in unwounded primary veins were *c.* 40-fold higher than those in the sheath (Fig. 1a). In wounded leaf 8, OPDA levels in the primary vein and vein sheath fell within 10 min and remained at low levels until 30 min postwounding (Fig. 1a). OPDA kinetics were similar in the primary vein of distal leaf 13, although they did not reach such low levels as seen in the primary vein of leaf 8 (Fig. 1a). Vascular jasmonic acid (JA) levels began increasing within < 3 min of wounding in both local and distal primary veins, reaching maxima *c.* 10 min after wounding (Fig. 1b).

JA-Ile levels also increased shortly after wounding, but while the concentrations kept increasing until 30 min in the wounded vein, they peaked at 10 min and then tended to decrease in the distal vein (Fig. 1c). JA-Ile levels in the vein sheath increased in response to wounding but were significantly lower than levels in veins from wounded plants (Fig. 1c).

LOX6 builds the pool of unbound OPDA in primary veins

Basal OPDA levels in the aerial tissues of *Arabidopsis* are strongly reduced in a *lox6* mutant relative to the wild-type (WT; Grebner *et al.*, 2013). Also, rapid changes in JA and JA-Ile levels in leaves distal to wounds were not observed in *lox6* mutants (Chauvin *et al.*, 2013). To test whether vascular OPDA production was LOX6-dependent, leaf 8 was wounded, and 10 min later, the primary vasculature was extracted from leaf 13. In response to wounding, the levels of OPDA decreased approximately fivefold in the primary veins of leaf 13 of the WT. In the *lox6B* mutant, OPDA basal levels were strikingly low compared with WT (Fig. S1a). In the *lox2-1 lox3B lox4A* triple mutant that carries a functional *LOX6* gene, OPDA levels in unwounded and wounded plants were similar to those of the WT. The *lox6B* mutant attenuated most of the wound-response increase in JA levels in the leaf 13 vein (Fig. S1b). Similarly, *lox6B* greatly reduced wound-induced increases in JA-Ile levels (Fig. S1c).

OPDA-MGMGs in primary veins

To address the question of whether wounding affects vascular pools of bound oxylipins, metabolite profiles from extracts of veins from undamaged plants were acquired using untargeted LC–MS (UHPLC-HRMS/MS performed in data-dependent acquisition mode using negative ionization). Four putative dnOPDA- and OPDA-bound lipids and two putative linolenic acid (18:3)-bound lipids were identified (Fig. 2a). All these compounds appeared as isomeric pairs with a common MGMG moiety. They were all detected as formate adducts $[M + HCOO]^-$ (*m/z*: 545.2630 for dnOPDA-MGMG, *m/z*: 573.2930 for OPDA-MGMG and *m/z*: 559.3120 for 18:3-MGMG) and exhibited a common neutral loss of 282 Da corresponding to the galactoglycerol + formate moiety and leading to the characteristic MS^2 fragments of dnOPDA/OPDA/18:3 respectively 263.1650, 291.1976 and 277.2172 (Table S2).

To determine whether dnOPDA-MGMGs and OPDA-MGMGs peaks corresponded to different regioisomers as proposed in Glauser *et al.* (2008), a targeted isolation strategy was established to purify these compounds for their *de-novo* structural identification by NMR (Fig. S2). Since MGMG levels and the amount of vein material were too low to generate sufficient amounts for structural elucidation, we explored alternative options and found that the levels of all forms were increased in leaves 30 minutes after wounding (Fig. S3). Two thousand five hundred leaves were wounded, extracted and fractionated by MPLC. Based on LC–MS analysis of individual fractions, all compounds of interest eluted between fraction (F) F96-F129 (Fig. S4). F97 contained a dnOPDA-MGMG isomer which was
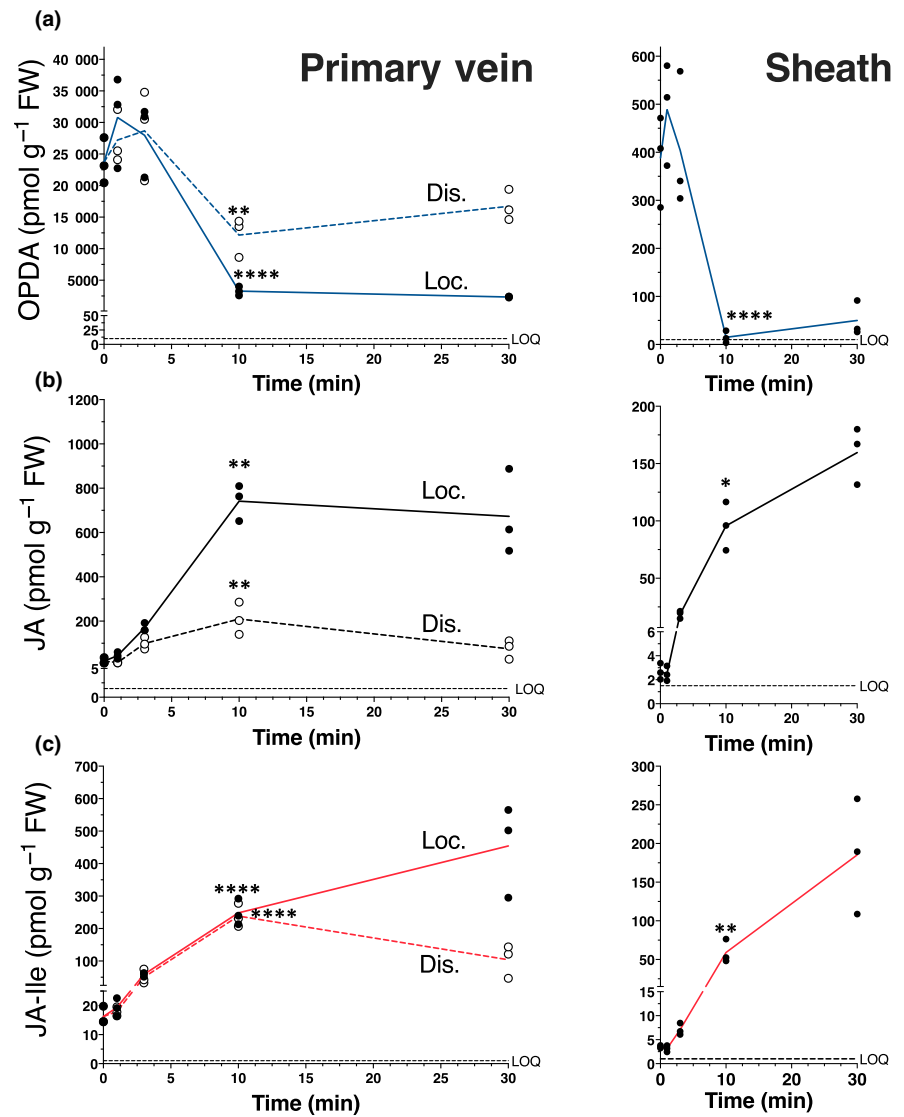
Fig. 1 Primary veins are reservoirs of 12-oxo-phytodienoic acid (OPDA). Early dynamics of free OPDA (a), jasmonic acid (JA) (b) and jasmonoyl-isoleucine (JA-Ile) (c) in primary veins and vein sheaths from the unwounded part of the damaged leaf 8 (Loc; solid lines) and in distal leaf 13 (Dis; dashed lines) in the wild-type (WT). Wounding was performed by mechanically crushing 30% of leaf 8 from the tip. The primary veins of leaf 8 and the primary veins of distal leaf 13 were analysed at 1, 3, 10 and 30 min after wounding leaf 8. At 0 min, unwounded veins (from leaves 8 to 11) were analysed. Each biological replicate was from pooled veins from at least five different rosettes. In the same time course, levels of free OPDA, JA and JA-Ile in the sheath tissue (lacking primary veins) from leaf 8 are shown in the right part. The data are from three biological replicates ±SD. Statistics are given only for the 10 min time point since this was used in many following experiments. Asterisks indicate data significantly different from WT unwounded veins (*, $P < 0.05$; **, $P < 0.01$; ****, $P < 0.0001$; t-test). Limits of quantification (LOQs) are indicated with dashed lines.

pure enough for structural elucidation using 1D and 2D NMR. This structure was identified as *sn*-2-dnOPDA-MGMG and corresponded to the major dnOPDA-MGMG form in primary veins (Fig. S5a; Notes S1; Tables S2, S3).

F118 and F119 (Fig. S4) contained an OPDA-MGMG isomer. 1D and 2D NMR analyses revealed that this was *sn*-1-*O*-(*cis*-12-oxo-phytodienoyl)-*sn*-3-*O*-(β-galactopyranosyl)glyceride (*sn*-1-OPDA-MGMG; Fig. S5a; Notes S1; Tables S2, S4). The LC–MS analysis of F116 indicated the presence of the other isomeric form of OPDA-MGMG. ^{1}H NMR analysis indicated that it was present in mixture with other metabolites from the wounded leaf extract. Comparison of 1D and 2D NMR spectra of *sn*-1-OPDA-MGMG and *sn*-2-dnOPDA-MGMG with the OPDA-MGMG isomer from F116 enabled its characterization as *sn*-2-*O*-(*cis*-12-oxo-phytodienoyl)-*sn*-3-*O*-(ß-galactopyranosyl) glyceride (*sn*-2-dnOPDA-MGMG; Fig. S5b; Notes S1, Table S2). *Sn*-2-OPDA-MGMG was far more abundant in veins than *sn*-1-OPDA-MGMG (Fig. 2a). Using ^{1}H NMR, we also characterized *sn*-2-18:3-MGMG (Fig. S6; Notes S1; Tables S2, S5).

Structures of the dominant vascular MGMG forms discovered are shown in Fig. 2(b). Although *sn*-2-OPDA-MGMG was the most abundant OPDA-MGMG form in veins, it was barely detectable in the *lox6* mutant (Fig. S7). By contrast, levels of *sn*-2-18:3-MGMG were similar in the WT and *lox6* (Fig. S7). To test whether oxygenated galactolipid levels changed up on leaf damage, veins were compared before and 10 min after wounding. The relative levels of both *sn*-2-OPDA-MGMG and *sn*-1-OPDA-MGMG decreased in veins distal to wounds (Fig. 3a). In subsequent experiments, we focused on the former, most abundant of the two molecules.

sn-2-OPDA-MGMG depletion is triggered by membrane depolarization

Slow-wave potential transmission from wounded leaves to distal leaves is blocked by mutating *GLUTAMATE RECEPTOR-LIKE* (*GLR*) genes *GLR3.3* and *GLR3.6* (Mousavi *et al.*, 2013). Oxylipin dynamics in the primary veins of a *glr3.3 glr3.6* double
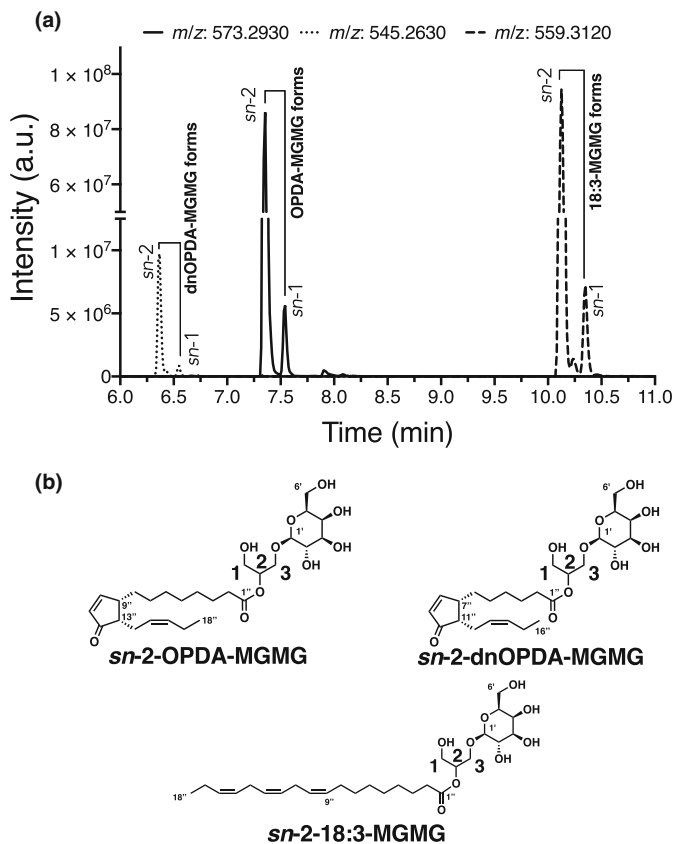
Fig. 2 MGMGs in the primary vasculature. (a) Superimposed extracted ion chromatograms (*m/z*: 545.2630, 559.3120, 573.2930) from UHPLC-HRMS metabolite profiling in negative ionization mode highlighting the chromatographic region corresponding to the elution of MGMGs forms in unwounded veins of wild-type (WT) plants. For each MGMG form detected, two isoforms were annotated corresponding to dnOPDA-MGMG (dotted line), OPDA-MGMG (solid line) and 18:3-MGMG (dashed line). (b) Structures of the major isomeric form of each MGMG contained in veins after characterization by NMR (Supporting Information Table S2). These forms were all esterified in the *sn*-2 position.

mutant and the WT after wounding were compared quantitatively. For this experiment, leaf 8 was wounded and, 10 min later, the primary vein of leaf 13 was extracted and analysed. In WT veins distal to wounds, and as expected (Koo *et al.*, 2009), OPDA levels fell within 10 min after wounding as had *sn*-2-OPDA-MGMG levels (Fig. 3b). By contrast, in the *glr3.3 glr3.6* double mutant OPDA and *sn*-2-OPDA-MGMG levels did not decrease after wounding. At the same time point, and consistent with a previous report (Chauvin *et al.*, 2013), JA and JA-Ile levels had increased in the distal veins of wounded WT plants. However, JA levels remained unchanged after wounding and JA-Ile levels were below the limit of quantification in both unwounded and wounded veins of *glr3.3 glr3.6* double mutant (Fig. 3b).

Acylhydrolases involved in vascular jasmonate precursor pool remodelling

In their broad survey of the effects of mutations in 18 acylhydrolases from the Arabidopsis phospholipase A (PLA) superfamily,

Ellinger *et al.* (2010) produced a quadruple mutant designated *c1x11*. This plant carries the following mutations: *dall1* (PLA-Iβ2, At4g16820), *dall2* (PLA-Iγ3, At1g51440), *dall3* (PLA-Iγ2, At2g30550) and *dall4* (PLA-Iγ1, At1g06800). Moreover, Ellinger *et al.* (2010) found that undamaged and wounded *c1x11* mutants had lower-than-WT levels of jasmonic acid (JA) and OPDA in their leaves. In Ellinger *et al.* (2010) entire wounded leaves were analysed for oxylipin contents. To test whether *c1x11* interfered with jasmonate signalling activation in leaves distal to wounds, we monitored the levels of the *JAZ10* transcript (Yan *et al.*, 2007) in leaf 13 1 h after wounding leaf 8. Wound-inducible *JAZ10* transcript levels in whole leaf 13 were lower in *c1x11* than in the WT (Fig. 4a). This means that one or several of the four acylhydrolases in *c1x11* are likely to act in jasmonate synthesis in leaves distal to wounds.

We next analysed free and bound oxylipins in veins distal to the wound in the WT and the *c1x11* quadruple mutant. These results revealed that the *c1x11* mutant had highly reduced basal levels of OPDA and *sn*-2-OPDA-MGMG compared with the WT and that wounding did not significantly change the levels of these two jasmonates and of JA and JA-Ile (Fig. 4b). Furthermore, the levels of *sn*-2-18:3-MGMG were also strongly reduced in the mutant (Fig. 4c). In the case of diacyl galactolipids (DGs), resting 18:3/18:3-MGDG and 18:3/16:3-MGDG levels were statistically similar in both genotypes (Fig. S8). This indicated that the mutation present in *c1x11* does not strongly affect all galactolipids.

Deconvolution of *c1x11*

The *dall* mutants used were genotyped (Fig. S9a), and both the *dall2* and *dall3* alleles used to produce the double mutant displayed reduced levels of their respective transcripts (Fig. S9b). Next, the impacts of the four individual *DALL* genes mutated in *c1x11* on *JAZ10* transcript levels in distal leaf 13 were examined 1 h after wounding leaf 8. At that time point, *JAZ10* transcript levels were increased in leaf 13 of the wounded WT. A slight increase in *JAZ10* transcripts relative to the WT was detected in wounded *dall1* (Fig. S10). However, wound-induced *JAZ10* transcript levels were similar in *dall2*, *dall3* and *dall4* relative to the WT. We then constructed *dall* double mutants. All T-DNA double mutants carrying *dall2* alleles showed reduced *JAZ10* transcript levels when compared to the WT (Fig. S11) and this effect was strongest in *dall2 dall3*. To verify these results, a second independent mutant termed *dall2c dall3c* was generated using CRISPR-Cas9 (Fig. S12). When *dall2c dall3c* was wounded, similar effects on *JAZ10* transcript induction to those obtained with the *dall2 dall3* T-DNA insertion mutant were obtained (Fig. 5a).

We extended these qPCR analyses to isolated veins from leaves distal to wounds. Again, levels of *JAZ10* transcripts were lower in the veins of wounded *dall2c dall3c* than in veins of the wounded WT (Fig. 5b). These results confirmed the roles of the two DALLs in jasmonate precursor production in leaves and veins distal to wounds. Vascular oxylipin levels in unwounded and wounded *dall2c dall3c* double mutants were then analysed. For these experiments, veins from distal leaf 13 were harvested
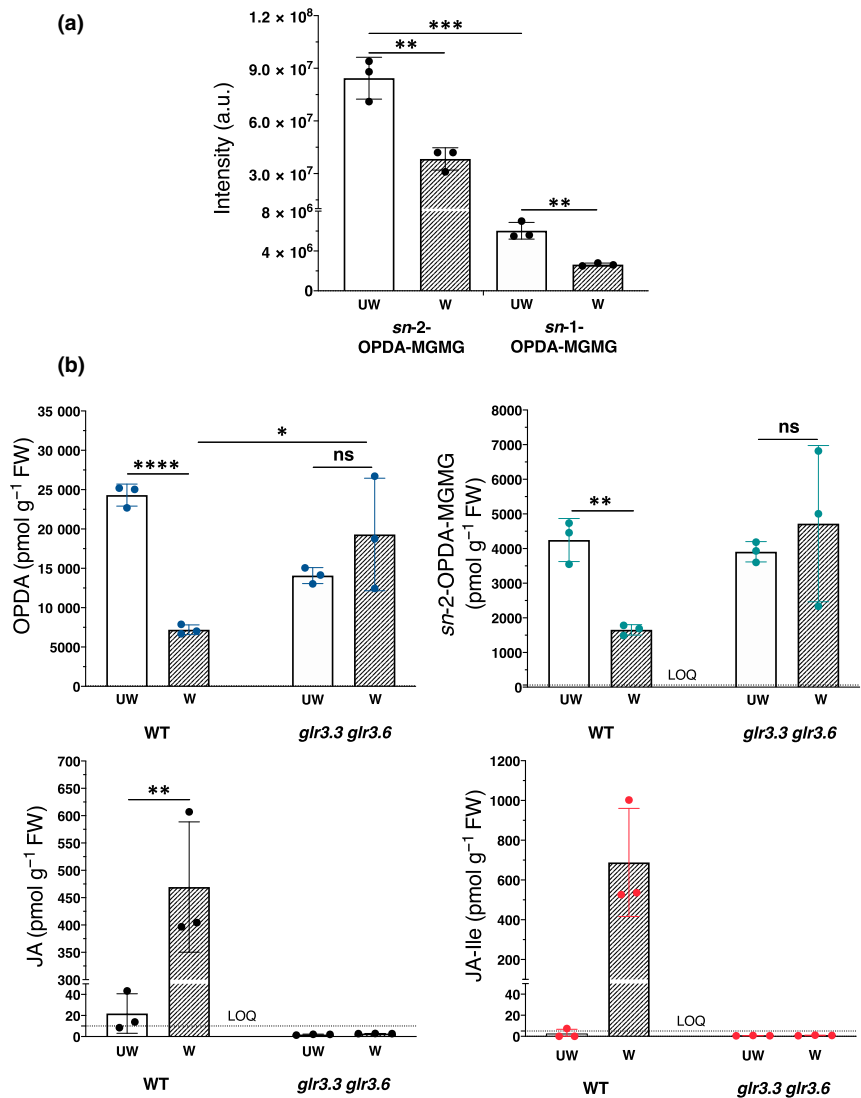
Fig. 3 Leaf-to-leaf electrical signals trigger 12-oxo-phytodienoic acid (OPDA) and OPDA-MGMG depletion in veins. (a) Semi-quantitative levels of *sn*-2-OPDA-MGMG (left part) and *sn*-1-OPDA-MGMG (right part) monitored by UHPLC-HRMS/MS. (b) Jasmonate levels in the primary vasculature of wounded wild-type (WT) plants and *glr3.3 glr3.6* double mutants were quantitated. Mechanical wounding was performed by crushing 30% of the tip of leaf 8. After 10 min, veins were extracted from leaf 13. Jasmonate levels in the wounded plants (W, hatched bars) were compared with unwounded plants (UW, white bars). Each biological replicate consisted of pooling veins from at least five different rosettes. The data are from three biological replicates ±SD. Asterisks indicate significant differences (**, $P < 0.01$; ***, $P < 0.001$; ****, $P < 0.0001$; t-test; ns, non-significant). Only data above the limit of quantification (LOQ, dotted lines) were suitable for statistical analysis.

10 min after wounding leaf 8. The *dall2* mutant was impaired in the production of basal levels of OPDA, *sn*-2-OPDA-MGMG and JA. In this same background, JA and its bioactive form, JA-Ile were slightly induced after wounding but their levels were far lower than those of the WT (Fig. 5c). Additionally, the levels of JA and JA-Ile in the wounded veins of *dall3* were higher than those of the WT. Dioxygenated linolenic acid (18:3) has been found in leaves (Buseman *et al.*, 2006) and might correspond to 18:3-hydroperoxide intermediates in jasmonate synthesis. Mutation of DALL2 or LOX6 attenuated dioxygenated 18:3 production (Fig. S13). While the formation of dioxygenated MGDGs was LOX6-dependent, it was DALL2/DALL3-independent (Fig. S14).

DALL2 protein localization

To explore DALL2 protein localization, a translational DALL2-β-glucuronidase (GUS) fusion was generated. GUS staining of whole leaves (Fig. 6a) revealed DALL2 associated with

the vasculature where it localized most strongly to the xylem contact cell region (Fig. 6b).

Discussion

Electrical signalling triggers vascular galactolipid remodelling

We performed metabolomic studies aimed at identifying early events leading to vascular JA-Ile synthesis provoked by wounding. In most experiments, leaf blade tissues which are sites for arabidopside production (Glauser *et al.*, 2009; Chauvin *et al.*, 2016) were discarded, and we focused on the primary vein. Buseman *et al.* (2006) reported increases in the levels of oxylipin-bound galactolipids in whole leaves 15 min after wounding. The vascular MGMGs reported herein differ from those identified by Buseman *et al.* (2006) and included the novel galactolipid *sn*-2-OPDA-MGMG. As is the case for OPDA (Chauvin *et al.*, 2013; Grebner *et al.*, 2013), the production of *sn*-2-OPDA-MGMG
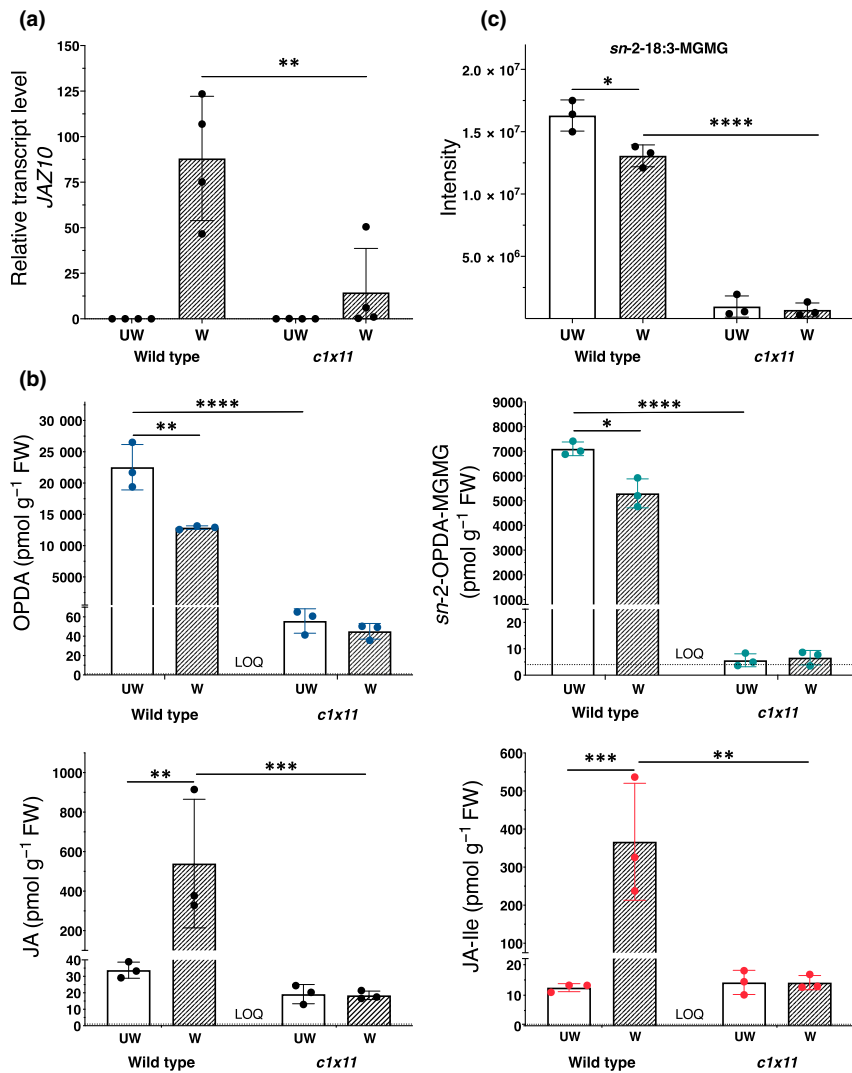
Fig. 4 Vascular jasmonate dynamics in the wounded *c1x11* quadruple mutant. (a) *JAZ10* transcript levels in whole leaf 13 1 h after wounding leaf 8 of the wild-type (WT) or *c1x11* mutant. Undamaged leaves 8–11 were used as unwounded controls. (b) Biochemical analyses of free 12-oxo-phytodienoic acid (OPDA), *sn*-2-OPDA-MGMG, jasmonic acid (JA) and jasmonoyl-isoleucine (JA-Ile) in the primary veins of the WT and the *c1x11* quadruple mutant. (c) *sn*-2-18:3-MGMG levels in the WT and *c1x11*. At 0 min, unwounded veins from leaves 8–11 were analysed. Ten minutes after wounding leaf 8, veins from leaf 13 were analysed. Each biological replicate consisted of pooling veins from at least five different rosettes. The data are from three biological replicates ±SD. Asterisks indicate significant differences (*, $P < 0.05$; **, $P < 0.01$; ***, $P < 0.001$; ****, $P < 0.0001$, *t*-test). Only data above the limit of quantification (LOQ, dotted lines) were suitable for statistical analysis. For all experiments, UW, unwounded; W, wounded.

required LOX6. *Sn*-2-dnOPDA-MGMG reported by Glauser *et al.* (2008) was also found in veins and its structure was confirmed herein using NMR. Additionally, *sn*-1-OPDA-MGMG and *sn*-1-dnOPDA-MGMG were detected in veins but were found to be roughly 10 times less abundant than the corresponding *sn*-2 forms. *Sn*-1-OPDA-MGMG occurs in the Asterid *Ipomoea tricolor* (Ohashi *et al.*, 2005) and in Arabidopsis, a Rosid (Glauser *et al.*, 2008), hinting at a possible broad occurrence in angiosperms. Whether *sn*-2-OPDA-MGMG is widespread in plants remains unknown. Upon wounding, the levels of *sn*-1-, *sn*-2-OPDA-MGMG and *sn*-2-18:3-MGMG in veins fell. Further quantitative analyses revealed that the combined decreases in OPDA, *sn*-2-OPDA-MGMG and *sn*-2-18:3-MGMG exceeded the increases in JA and JA-Ile levels. Therefore, OPDA and MGMG depletion may serve not only for jasmonate production and might have additional purposes. A dioxygenase that modifies OPDA, reducing its conversion to JA-Ile, has been reported (Yi *et al.*, 2023). Wound-response decreases in OPDA, *sn*-2-OPDA-MGMG and *sn*-2-18:3-MGMG did not occur in the wounded *glr3.3 glr3.6* double mutant, which cannot propagate electrical signals to leaves distal to damage sites. We

conclude that extensive electrical signal-dependent remodelling of chloroplast galactolipids takes place in primary veins during wound-response jasmonate synthesis.

When compared to the WT, the *c1x11* quadruple mutant produced by Ellinger *et al.* (2010) displayed reduced *JAZ10* transcript levels in leaf 13 when leaf 8 was wounded. Among the genes mutated in *c1x11*, *DALL2* was a candidate for roles in foliar jasmonate synthesis (Ellinger *et al.*, 2010; Lin *et al.*, 2016). However, reduced function mutations in *DALL2* alone did not strongly affect *JAZ10* expression in leaves distal to wounds. Instead, we found that T-DNA insertion *dall2 dall3* mutants reduced distal jasmonate signalling and this observation was verified by producing the *dall2c dall3c* using CRISPR-Cas9. Metabolomic analyses revealed that *dall2c dall3c* attenuated vascular wound-response JA-Ile synthesis, and this was also found to be the case for *dall2* single mutants. Importantly, our results do not explain why *dall2* single mutants, which display similar wound-response levels of JA-Ile to those of *dall2 dall3*, display higher levels of *JAZ10* transcription than those of the double mutant. Different time points were used to harvest tissues for oxylipin and *JAZ10* analyses, so this may in part be responsible. However,
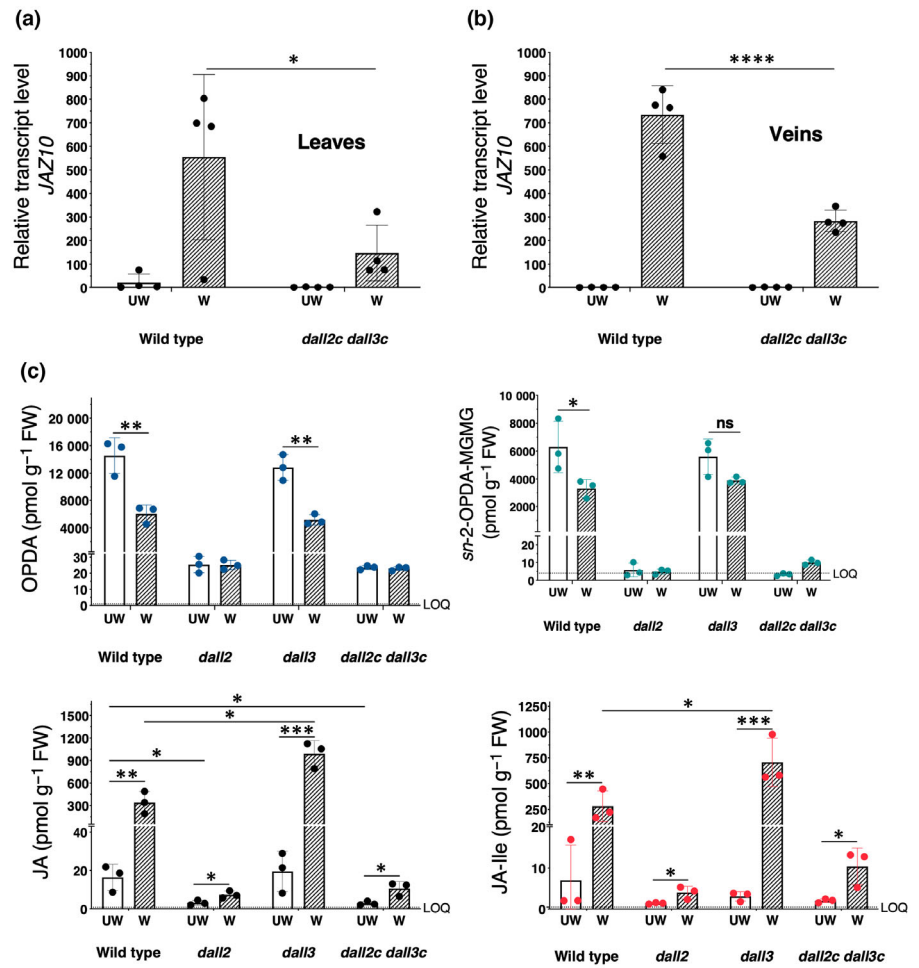
Fig. 5 *dall2c dall3c* attenuates *JAZ10* expression and jasmonoyl-isoleucine (JA-Ile) accumulation in veins distal to wounds. (a) *JAZ10* expression in whole leaf 13 of the wild-type (WT) or *dall2c dall3c* 1 h after wounding leaf 8 or in unwounded leaves 8–11. (b) *JAZ10* expression in primary veins isolated from leaf 13 1 h after wounding leaf 8 or in control. (c) Metabolite levels in primary veins of the WT, *dall2(30)*, *dall3* and *dall2c dall3c* plants. For metabolite analyses, veins were isolated from leaf 13 10 min after wounding leaf 8. UW, unwounded; W, wounded. Asterisks indicate significant differences (*, $P < 0.05$; **, $P < 0.01$; ***, $P < 0.001$; ****, $P < 0.0001$; *t*-test; ±SD). Only data above the limit of quantification (LOQ, dotted lines close to the abscissa) were suitable for statistical analysis.
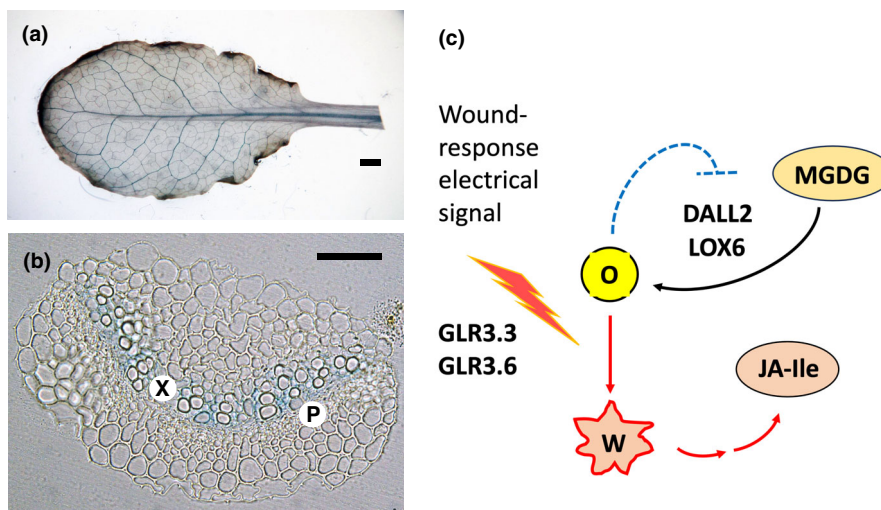

Fig. 6 DALL2 function in xylem contact cells. (a) Localization of DALL2-GUS fusion protein in a rosette leaf. Bar, 1 mm. (b) Localization of DALL2-GUS in the primary vasculature. X, xylem region; P, phloem region. Note DALL2 association with the xylem region. Bar, 50 μm. (c) Speculative model illustrating one potential scenario for LOX6/DALL2 interdependent jasmonate precursor synthesis. LOX6 and DALL2 together produce oxygenated lipids (O) including OPDA-MGMGs and OPDA from MGDG (and possibly oxygenated 18:3). The possibility that these intermediates inhibit excess DALL2/LOX6 action is indicated (dashed line). Upon wounding, GLR3.3/GLR3.6-dependent electrical signals trigger phase changes in populations of O converting them to different phases (W). This allows JA-Ile production.

it is possible that mechanisms other than JA-Ile concentrations impinge on the control of *JAZ10* expression.

DALL function in vascular jasmonate synthesis

Our findings concerning DALL2 can be summarized as follows: DALL2 is necessary for rapid jasmonate synthesis in veins distal to wounds. In the veins of unwounded plants, both OPDA and *sn*-2-OPDA-MGMG levels are strongly reduced in *dall2* relative to the WT. Similar to Buseman *et al.* (2006), we found oxygenated 18:3 species. It was notable that both *lox6* and *dall2* mutants caused reduced levels of dioxygenated galactolipids. An apparent exception was *sn*-1-hydroperoxy-18:3-MGDG. Nakashima *et al.* (2011) identified this compound as a product of soybean LOX1. We found fragments typical of this molecule in Arabidopsis and discovered that its production was LOX6-dependent but DALL2/3-independent (Fig. S14). MGDG is a preferred substrate for DALL2 and DALL3, which catalyse glycerolipid hydrolysis at the *sn*-1 position *in vitro* (Seo *et al.*, 2009). Our results do not clarify which molecules (OPDA, OPDA-MGMGs or others) are substrates for JA-Ile synthesis. We note that if *sn*-2-OPDA-MGMG was used as a substrate for OPDA synthesis, *sn*-2 hydrolytic activity would be needed to free OPDA from this galactolipid. How DALL3 prevents the accumulation of higher-than-WT levels of JA and JA-Ile in wounded plants is unknown. However, given the similar enzymatic activities of DALL2 and DALL3 (Seo *et al.*, 2009), the latter might, in theory, compete for lipids which are substrates for DALL2. While our results tell us nothing about DALL4 function, there is slightly enhanced *JAZ10* expression in leaves of *dall1* distal to wounds. Similarly to DALL3, DALL1 might act to modulate jasmonate pathway activity (Fig. S10).

Leaf wounding initiates rapid LOX6-dependent JA-Ile synthesis in xylem contact cells (Gasperini *et al.*, 2015), and we herein localized DALL2 to the same cells. We also note that *DALL3* promoter activity in Arabidopsis is associated with the xylem (Dervisi *et al.*, 2020). These findings provide a cellular context for membrane depolarization-triggered galactolipid remodelling. In summary, our three main findings were (1) electrical signal-dependent remodelling of vascular galactolipid pools, (2) the discovery of *sn*-2-OPDA-MGMG, and (3) the apparently interdependent action of DALL2 and LOX6 in the production of several oxygenated galactolipids including *sn*-2-OPDA-MGMG and OPDA. We attempt to summarize these findings in Fig. 6c.

Perspectives

Chloroplast MGDG/DGDG ratios help to determine thylakoid packing (Mazur *et al.*, 2019). Moreover, increased MGDG/DGDG ratios in the *dgdg synthase 1*(*dgd1*) mutant lead to spontaneous jasmonate synthesis (Lin *et al.*, 2016; Yu *et al.*, 2020). Although the unwounded *c1x11* mutant has higher MGDG levels than the WT (Fig. S8), the mutant produces lower JA-Ile levels than the wounded WT. This opens the possibility that other mechanisms operate to control wound-response jasmonate synthesis. What could these mechanisms be? We suggest that lipid phase changes may play roles in the membrane

depolarization-triggered initiation of jasmonate synthesis. Seo *et al.* (2009) reported that the hydrolysis of MGDG *in vitro* by DALL2 (and to a lesser extent, DALL3) is inhibited by the detergent Triton X100. Subsequently, Wang *et al.* (2018) pointed out the potential detergent-like properties of OPDA. Interestingly, MGMGs form non-bilayer, hexagonal phases (Demé *et al.*, 2014) that are strongly sensitive to changes in pH, ionic strength and osmolarity (Garab *et al.*, 2017). Each of these parameters may change upon membrane depolarization, and MGMGs including *sn*-2-OPDA-MGMG are of potential interest in this respect. Electrical signals might cause phase changes in OPDA-MGMGs and other MGMG forms, thereby enabling rapid wound-response jasmonate synthesis in xylem contact cells. Given the complexity of the present findings, future *in vitro* studies on the catalytic activities of LOX6 and DALL2 in the presence of OPDA-MGMGs and OPDA would be warranted.

Competing interests

None declared.

Author contributions

HM, GG and LM performed analytical experiments. AC and SS produced *dall* mutants and performed genotyping and qPCRs. AC carried out DALL localization experiments. HM, J-LW and EEF analysed the data. EEF, HM and J-LW wrote the paper. EEF agrees to serve as the author responsible for contact. This work was supported by Swiss National Science Foundation grants 31003A_163424 (to J-LW and EEF) and 31003A_175566 (to EEF).

ORCID

Aurore Chételat https://orcid.org/0000-0001-5470-6242
Edward E. Farmer https://orcid.org/0000-0002-6572-5024
Gaëtan Glauser https://orcid.org/0000-0002-0983-8614
Laurence Marcourt https://orcid.org/0000-0002-9614-1099
Hugo Morin https://orcid.org/0000-0003-3969-2406
Stéphanie Stolz https://orcid.org/0000-0002-5267-0722
Jean-Luc Wolfender https://orcid.org/0000-0002-0125-952X

Data availability

The data that support the findings of this study are available in the Supporting Information for this article.

References

Acosta IF, Gasperini D, Chételat A, Stolz S, Santuari L, Farmer EE. 2013. Role of NINJA in root jasmonate signaling. *Proceedings of the National Academy of Sciences, USA* **110**: 15473–15478.

Buseman CM, Tamura P, Sparks AA, Baughman EJ, Maatta S, Zhao J, Roth MR, Esch SW, Shah J, Williams TD et al. 2006. Wounding stimulates the accumulation of glycerolipids containing oxophytodienoic acid and dinor-oxophytodienoic acid in Arabidopsis leaves. *Plant Physiology* **142**: 28–39.

Caldelari D, Wang G, Farmer EE, Dong X. 2011. Arabidopsis *lox3 lox4* double mutants are male sterile and defective in global proliferative arrest. *Plant Molecular Biology* **75**: 25–33.

Challal S, Queiroz E, Debrus B, Kloeti W, Guillarme D, Gupta M, Wolfender J-L. 2015. Rational and efficient preparative isolation of natural products by MPLC-UV-ELSD based on HPLC to MPLC gradient transfer. *Planta Medica* **81**: 1636–1643.

Chauvin A, Caldelari D, Wolfender J, Farmer EE. 2013. Four 13-lipoxygenases contribute to rapid jasmonate synthesis in wounded *Arabidopsis thaliana* leaves: a role for lipoxygenase 6 in responses to long-distance wound signals. *New Phytologist* **197**: 566–575.

Chauvin A, Lenglet A, Wolfender J-L, Farmer E. 2016. Paired hierarchical organization of 13-lipoxygenases in *Arabidopsis*. *Plants* **5**: 16.

Demé B, Cataye C, Block MA, Maréchal E, Jouhet J. 2014. Contribution of galactoglycerolipids to the 3-dimensional architecture of thylakoids. *The FASEB Journal* **28**: 3373–3383.

Dervisi I, Valassakis C, Agalou A, Papandreou N, Podia V, Haralampidis K, Iconomidou VA, Kouvelis VN, Spaink HP, Roussis A. 2020. Investigation of the interaction of DAD1-LIKE LIPASE 3 (DALL3) with selenium binding protein 1 (SBP1) in *Arabidopsis thaliana*. *Plant Science* **291**: 110357.

Ellinger D, Stingl N, Kubigsteltig II, Bals T, Juenger M, Pollmann S, Berger S, Schuenemann D, Mueller MJ. 2010. DONGLE and DEFECTIVE IN ANTHER DEHISCENCE1 lipases are not essential for wound- and pathogen-induced jasmonate biosynthesis: redundant lipases contribute to jasmonate formation. *Plant Physiology* **153**: 114–127.

Erb M, Reymond P. 2019. Molecular interactions between plants and insect herbivores. *Annual Review of Plant Biology* **70**: 527–557.

Farmer EE, Kurenda A. 2018. Rapid extraction of living primary veins from the leaves of *Arabidopsis thaliana*. *Protocol Exchange*. doi: 10.1038/protex.2018. 119.

Fonseca S, Chini A, Hamberg M, Adie B, Porzel A, Kramell R, Miersch O, Wasternack C, Solano R. 2009. (+)-7-iso-Jasmonoyl-L-isoleucine is the endogenous bioactive jasmonate. *Nature Chemical Biology* **5**: 344–350.

Garab G, Ughy B, Waard PD, Akhtar P, Javornik U, Kotakis C, Šket P, Karlický V, Materová Z, Špunda V et al. 2017. Lipid polymorphism in chloroplast thylakoid membranes – as revealed by ^{31}P-NMR and time-resolved merocyanine fluorescence spectroscopy. *Scientific Reports* **7**: 13343.

Gasperini D, Chauvin A, Acosta IF, Kurenda A, Stolz S, Chetelat A, Wolfender J-L, Farmer EE. 2015. Axial and radial oxylipin transport. *Plant Physiology* **169**: 2244–2254.

Genva M, Obounou Akong F, Andersson MX, Deleu M, Lins L, Fauconnier M-L. 2019. New insights into the biosynthesis of esterified oxylipins and their involvement in plant defense and developmental mechanisms. *Phytochemistry Reviews* **18**: 343–358.

Gfeller A, Baerenfaller K, Loscos J, Chételat A, Baginsky S, Farmer EE. 2011. Jasmonate controls polypeptide patterning in undamaged tissue in wounded arabidopsis leaves. *Plant Physiology* **156**: 1797–1807.

Glauser G, Dubugnon L, Mousavi SAR, Rudaz S, Wolfender J-L, Farmer EE. 2009. Velocity estimates for signal propagation leading to systemic jasmonic acid accumulation in wounded *Arabidopsis*. *Journal of Biological Chemistry* **284**: 34506–34513.

Glauser G, Grata E, Rudaz S, Wolfender J-L. 2008. High-resolution profiling of oxylipin-containing galactolipids in Arabidopsis extracts by ultra-performance liquid chromatography/time-of-flight mass spectrometry: profiling of oxylipin-containing galactolipids in Arabidopsis. *Rapid Communications in Mass Spectrometry* **22**: 3154–3160.

Glauser G, Vallat A, Balmer D. 2014. Hormone profiling. In: Sanchez-Serrano JJ, Salinas J, eds. *Methods in molecular biology*. Arabidopsis *protocols*. Totowa, NJ, USA: Humana Press, 597–608.

Grebner W, Stingl NE, Oenel A, Mueller MJ, Berger S. 2013. Lipoxygenase6-dependent oxylipin synthesis in roots is required for abiotic and biotic stress resistance of Arabidopsis. *Plant Physiology* **161**: 2159–2170.

Hause B, Hause G, Kutter C, Miersch O, Wasternack C. 2003. Enzymes of jasmonate biosynthesis occur in tomato sieve elements. *Plant and Cell Physiology* **44**: 643–648.

Hölzl G, Dörmann P. 2007. Structure and function of glycoglycerolipids in plants and bacteria. *Progress in Lipid Research* **46**: 225–243.

Howe GA, Major IT, Koo AJ. 2018. Modularity in jasmonate signaling for multistress resilience. *Annual Review of Plant Biology* **69**: 387–415.

Ishiguro S, Kawai-Oda A, Ueda J, Nishida I, Okada K. 2001. The *DEFECTIVE IN ANTHER DEHISCENCE1* gene encodes a novel phospholipase a1 catalyzing the initial step of jasmonic acid biosynthesis, which synchronizes pollen maturation, anther dehiscence, and flower opening in Arabidopsis. *Plant Cell* **13**: 2191–2209.

Jimenez Aleman GH, Thirumalaikumar VP, Jander G, Fernie AR, Skirycz A. 2022. OPDA, more than just a jasmonate precursor. *Phytochemistry* **204**: 113432.

Kimberlin AN, Holtsclaw RE, Zhang T, Mulaudzi T, Koo AJ. 2022. On the initiation of jasmonate biosynthesis in wounded leaves. *Plant Physiology* **189**: 1925–1942.

Koo AJK, Gao X, Daniel Jones A, Howe GA. 2009. A rapid wound signal activates the systemic synthesis of bioactive jasmonates in Arabidopsis. *The Plant Journal* **59**: 974–986.

Kurenda A, Nguyen CT, Chételat A, Stolz S, Farmer EE. 2019. Insect-damaged *Arabidopsis* moves like wounded *Mimosa pudica*. *Proceedings of the National Academy of Sciences, USA* **116**: 26066–26071.

Lin Y-T, Chen L-J, Herrfurth C, Feussner I, Li H. 2016. Reduced biosynthesis of digalactosyldiacylglycerol, a major chloroplast membrane lipid, leads to oxylipin overproduction and phloem cap lignification in Arabidopsis. *Plant Cell* **28**: 219–232.

Mazur R, Mostowska A, Szach J, Gieczewska K, Wójtowicz J, Bednarska K, Garstka M, Kowalewska Ł. 2019. Galactolipid deficiency disturbs spatial arrangement of the thylakoid network in *Arabidopsis thaliana* plants. *Journal of Experimental Botany* **70**: 4689–4704.

Mousavi SAR, Chauvin A, Pascaud F, Kellenberger S, Farmer EE. 2013. *GLUTAMATE RECEPTOR-LIKE* genes mediate leaf-to-leaf wound signalling. *Nature* **500**: 422–426.

Nakashima A, Iijima Y, Aoki K, Shibata D, Sugimoto K, Takabayashi J, Matsui K. 2011. Monogalactosyl diacylglycerol is a substrate for lipoxygenase: its implications for oxylipin formation directly from lipids. *Journal of Plant Interactions* **6**: 93–97.

Nilsson AK, Fahlberg P, Ellerström M, Andersson MX. 2012. Oxo-phytodienoic acid (OPDA) is formed on fatty acids esterified to galactolipids after tissue disruption in *Arabidopsis thaliana*. *FEBS Letters* **586**: 2483–2487.

Ohashi T, Ito Y, Okada M, Sakagami Y. 2005. Isolation and stomatal opening activity of two oxylipins from *Ipomoea tricolor*. *Bioorganic & Medicinal Chemistry Letters* **15**: 263–265.

Oñate-Sánchez L, Vicente-Carbajosa J. 2008. DNA-free RNA isolation protocols for *Arabidopsis thaliana*, including seeds and siliques. *BMC Research Notes* **1**: 93.

Ruduś I, Terai H, Shimizu T, Kojima H, Hattori K, Nishimori Y, Tsukagoshi H, Kamiya Y, Seo M, Nakamura K et al. 2014. Wound-induced expression of *DEFECTIVE IN ANTHER DEHISCENCE1* and DAD1-like lipase genes is mediated by both *CORONATINE INSENSITIVE1*-dependent and independent pathways in *Arabidopsis thaliana*. *Plant Cell Reports* **33**: 849–860.

Ryu SB. 2004. Phospholipid-derived signaling mediated by phospholipase A in plants. *Trends in Plant Science* **9**: 229–235.

Seo YS, Kim EY, Kim JH, Kim WT. 2009. Enzymatic characterization of class I DAD1-like acylhydrolase members targeted to chloroplast in *Arabidopsis*. *FEBS Letters* **583**: 2301–2307.

Shimada TL, Shimada T, Hara-Nishimura I. 2010. A rapid and non-destructive screenable marker, FAST, for identifying transformed seeds of *Arabidopsis thaliana*. *The Plant Journal* 61: 519–528.

Stahlberg R, Cleland RE, Van Volkenburgh E. 2006. Slow wave potentials – a propagating electrical signal unique to higher plants. In: Baluška F, Mancuso S, Volkmann D, eds. *Communication in plants*. Berlin, Heidelberg, Germany: Springer Berlin Heidelberg, 291–308.

Staswick PE, Tiryaki I. 2004. The oxylipin signal jasmonic acid is activated by an enzyme that conjugates it to isoleucine in Arabidopsis. *Plant Cell* 16: 2117–2127.

Stelmach BA, Müller A, Hennig P, Gebhardt S, Schubert-Zsilavecz M, Weiler EW. 2001. A novel class of oxylipins, *sn*1-*O*-(12-Oxophytodienoyl)-*sn*2-*O*-(hexadecatrienoyl)-monogalactosyl diglyceride, from *Arabidopsis thaliana*. *Journal of Biological Chemistry* 276: 12832–12838.

Ursache R, Fujita S, Dénervaud Tendon V, Geldner N. 2021. Combined fluorescent seed selection and multiplex CRISPR/Cas9 assembly for fast generation of multiple *Arabidopsis* mutants. *Plant Methods* 17: 111.

Wang J, Wu D, Wang Y, Xie D. 2019. Jasmonate action in plant defense against insects. *Journal of Experimental Botany* 70: 3391–3400.

Wang K, Guo Q, Froehlich JE, Hersh HL, Zienkiewicz A, Howe GA, Benning C. 2018. Two abscisic acid-responsive plastid lipase genes involved in jasmonic acid biosynthesis in *Arabidopsis thaliana*. *Plant Cell* 30: 1006–1022.

Wasternack C, Feussner I. 2018. The oxylipin pathways: biochemistry and function. *Annual Review of Plant Biology* 69: 363–386.

Weber H, Vick BA, Farmer EE. 1997. Dinor-oxo-phytodienoic acid: a new hexadecanoid signal in the jasmonate family. *Proceedings of the National Academy of Sciences, USA* 94: 10473–10478.

Yan Y, Stolz S, Chételat A, Reymond P, Pagni M, Dubugnon L, Farmer EE. 2007. A downstream mediator in the growth repression limb of the jasmonate pathway. *Plant Cell* 19: 2470–2483.

Yang W, Devaiah SP, Pan X, Isaac G, Welti R, Wang X. 2007. AtPLAI is an acyl hydrolase involved in basal jasmonic acid production and *arabidopsis* resistance to *Botrytis cinerea*. *Journal of Biological Chemistry* 282: 18116–18128.

Yi R, Du R, Wang J, Yan J, Chu J, Yan J, Shan X, Xie D. 2023. Dioxygenase JID1 mediates the modification of OPDA to regulate jasmonate homeostasis. *Cell Discovery* 9: 39.

Yu C, Lin Y, Li H. 2020. Increased ratio of galactolipid MGDG: DGDG induces jasmonic acid overproduction and changes chloroplast shape. *New Phytologist* 228: 1327–1335.

Supporting Information

Additional Supporting Information may be found online in the Supporting Information section at the end of the article.

Fig. S1 LOX6-dependent OPDA pools in the primary vasculature.

Fig. S2 Targeted isolation workflow.

Fig. S3 MGMG levels in unwounded veins and wounded leaves (30 min) of WT.

Fig. S4 MPLC-UV fractionation of methanolic extract from wounded leaves.

Fig. S5 OPDA-MGMG and dnOPDA-MGMG regiochemistry determination.

Fig. S6 *sn*-2-18:3-MGMG isolated from the primary vasculature.

Fig. S7 *sn*-2-OPDA-MGMG formation in primary veins is LOX6-dependent.

Fig. S8 MGDGs levels in the veins of the WT and *c1x11*.

Fig. S9 *dall* mutant genotyping and gene expression.

Fig. S10 Jasmonate-responsive gene expression in *dall* single mutants.

Fig. S11 Jasmonate-responsive gene expression in *dall* double mutants.

Fig. S12 Generation of the CRISPR-Cas9 *dall2c dall3c* double mutant.

Fig. S13 DALL2- and LOX6 dependent formation of 18-carbon dioxygenated fatty acids.

Fig. S14 DALL2/DALL3-independent formation of dioxygenated MGDGs in primary veins.

Notes S1 Details for structural elucidation of MGMGs.

Table S1 Primers for *dall* mutant genotyping.

Table S2 LC-HRMS and NMR data for the structural identification of MGMGs.

Table S3 ^{1}H NMR (recorded at 600 MHz in MeOD) and ^{13}C (recorded at 151 MHz in MeOD) chemical shifts for *sn*-2-dnOPDA- MGMG.

Table S4 ^{1}H NMR (recorded at 600 MHz in MeOD) and ^{13}C (recorded at 151 MHz in MeOD) chemical shifts for *sn*-1-OPDA-MGMG.

Table S5 ^{1}H NMR (recorded at 600 MHz in MeOD) chemical shifts for *sn*-2-18:3-MGMG.

Please note: Wiley is not responsible for the content or functionality of any Supporting Information supplied by the authors. Any queries (other than missing material) should be directed to the *New Phytologist* Central Office.